INTERNATIONAL JOURNAL OF
COASTAL & OFFSHORE ENGINEERING
IJCOE Vol.4/No. 2/Summer 2019 (1-9)

Available online at: http://ijcoe.org/browse.php?a_code=A-10-89-2&sid=1&slc_lang=en

Numerical Study on Wave Induced Flow Field around a Vibrant Monopile Regarding Cross-Sectional Shape

Mohammad Mohammad Beigi Kasvaei[1], Mohammad Hossein Kazeminezhad[2*], Abbas Yeganeh-Bakhtiary[3]

[1] *PhD Candidate, Iranian National Institute for Oceanography & Atmospheric Science, Tehran, Iran; mmbeigi@inio.ac.ir*
[2*] *Corresponding Author: Assistant Professor, Iranian National Institute for Oceanography & Atmospheric Science, Tehran, Iran; mkazeminezhad@inio.ac.ir*
[3] *Associate Professor, School of Civil Engineering, IUST, Tehran, Iran; yeganeh@iust.ac.ir*

ARTICLE INFO

Article History:
Received: 8 Jul. 2019
Accepted: 24 Aug. 2019

Keywords:
OpenFOAM®
RANS Equations
Vortex Induced Vibration (VIV)
Lock-in
Mesh deformation

ABSTRACT

A three-dimensional numerical simulation of regular waves passing over a monopile with square and circular cross-sectional shape was carried out to investigate flow field and vortex induced vibration. The rectangular wave flume and monopile are modeled with a solver; available in the open-source CFD toolkit OpenFOAM®. This solver applies the Reynolds-Averaged Navier-Stokes (RANS) equations with the volume of fluid technic (VOF) for tracking free surface. The motion equation together with mesh deformation was applied to capture monopile displacement. To validate the numerical model, results were compared to experimental data, and an admissible agreement was seen.

Computations were conducted for four cases with two different wave characteristics and different Keulegan-Carpenter (KC) numbers for square and circular cross-sectional shape. Vorticity field and *Q* criterion around the square and circular pile were depicted. It was seen that when KC increased, the difference in vortices around the square and the circular pile was more distinct. Investigations continued on transverse force coefficient and its oscillations. It was seen that by increasing KC, this coefficient and its frequency increased. When KC=20, the lift coefficient is larger for square pile compared to the circular pile. For both square and circular cross-sectional shape, the number of pile oscillation increased by increasing KC number. Also, the Strouhal number and vortex shedding frequency were larger for the circular pile compared to that of the square pile in vortex shedding regime. However, cross-flow vibration frequencies of the square and circular pile were close together.

1. Introduction

Wind turbines are nowadays one of the most used offshore structures in renewable energy equipment. A significant part of the wind turbine design process is related to its foundation design. A large number of marine structures such as offshore wind turbine are supported by a monopile foundation. Because of the presence of the pile, the wave-induced flow field around the pile changes and some vortices are generated. Dynamics of vortices depends on the cross-sectional shape of the pile and also on the wave characteristics, which can be stated by Keulegan-Carpenter number (KC):

$$\mathrm{KC} = \frac{U_m T}{D} \tag{1}$$

where the U_m is the maximum of the wave orbital velocity, T is the wave period, and D is the pile equivalent diameter. In addition to KC number, the cross-sectional shape of the pile influences on vortices pattern and its magnitude. Moreover, oscillating forces act on the pile due to the generated vortices around it when a pile is subjected to ocean waves. Elastically mounted pile subjected to the oscillating forces leads to so-called vortex induced vibration (VIV) of the pile. This vibration may lead to

increasing the fatigue loads and that is why it has been constantly considered in wave pile interaction issues.

A wide range of studies has been carried out in wave-pile interaction in a stationary or dynamic state of the pile. Sarpkaya and Rajabi [1], Zedan et al. [2], Angrilli and Cossalter [3], Bearman [4], Griffin [5], And Blevins [6] investigated extensively on the interaction of steady current and wave with pile during recent decades. Sumer and Fredsoe [7] carried out vast experimental studies of flow passing over vertical cylinders as well as wave-induced vortex shedding around the vertical pile. They used a range of different KC number to investigate its influence on different parameters around the pile such as vortices or force coefficients. Downes and Rockwell [8] studied the vibration of cylinders in wave experimentally. Many numerical studies on this subject have been implemented in recent years as well. Mo et al. [9], Jacobson et al. [10] and kasvaei et al. [11] simulated wave and a stationary pile interaction. Lou et al. [12] carried out a numerical study on vortex induced vibration of a marine riser. Zhao and Cheng [13] conducted a numerical investigation on vortex induced vibration of a circular cylinder of finite length subjected to uniform steady currents. Short literature review revealed that many studies have been conducted on VIV. Most of them, however, were about too slender cylindrical members such as marine risers. Also KC number, as an influencing parameter in wave-pile interaction problems, has not been purposefully considered.

The main aim of this paper is to investigate cross-sectional shape and KC number impact on the flow field around a vibrant monopile and on its dynamic response. Due to that, simulation of non-breaking regular waves passed over the vibrant monopile is carried out. Simulations have been performed for two different KC numbers to consider varying vortex shedding regimes.

The robust open source CFD code of OpenFOAM® with a multiphase, Eulerian solver (interDyMFoam) is applied. Mesh deformation is a capability of the solver to consider the pile displacement during vibration. Governing equations of the flow field and pile displacement are solved by finite volume discretization schemes in the code. Dynamics of vortex around the pile and vortex-induced vibration of the pile is investigated objectively regarding the influence of cross-sectional shape and KC number.

2. Numerical Model

2.1. Governing Equations

The incompressible fluid flow can be expressed by the 3D Reynolds averaged Navier-Stokes (RANS) equations with the continuity equation. These equations were used in the Cartesian coordinate system as the governing equations to find the flow field.

$$\frac{\partial U_i}{\partial t}+\frac{\partial\left(U_i U_j\right)}{\partial x_i} = -\frac{1}{\rho}\frac{\partial P}{\partial x_i}+\frac{\partial}{\partial x_i}\left[\frac{\mu_{eff}}{\rho}\left(\frac{\partial U_i}{\partial x_j}+\frac{\partial U_j}{\partial x_i}\right)\right]+g_i-\frac{\partial\left(\overline{u_i' u_j'}\right)}{\partial x_j} \quad (2)$$

$$\frac{\partial U_i}{\partial x_i}=0 \quad (3)$$

where U_i denotes the mean fluid velocity component in the i-th direction, P is the pressure, ρ is the fluid density, g_i denotes the acceleration of gravity, u' denotes the fluctuating velocity component, $\mu_{eff}=\mu+\mu_t$, μ is the molecular viscosity, and μ_t is the turbulent eddy viscosity.

To close the equations the Shear Stress Transport (SST) k-ω turbulence model was employed [14]. k as the turbulent kinetic energy with ω as the specific dissipation rate are expressed as:

$$\frac{\partial(\rho k)}{\partial t}+\frac{\partial\left(\rho U_j k\right)}{\partial x_j}=P_k-\beta^*\rho\omega k+\frac{\partial}{\partial x_j}\left[\left(\mu+\sigma_k\mu_t\right)\frac{\partial k}{\partial x_j}\right] \quad (4)$$

$$\frac{\partial(\rho\omega)}{\partial t}+\frac{\partial\left(\rho U_j\omega\right)}{\partial x_j}=\frac{\gamma}{\upsilon_t}P_k-\beta\rho\omega^2+\frac{\partial}{\partial x_j}\left[\left(\mu+\sigma_k\mu_t\right)\frac{\partial\omega}{\partial x_j}\right]+2\left(1-F_1\right)\frac{\rho\sigma_{\omega 2}}{\omega}\frac{\partial k}{\partial x_j}\frac{\partial\omega}{\partial x_j} \quad (5)$$

where F_1 is a harmonic function that is expressed as:

$$F_1=\tanh\left\{\min\left[\max\left(\frac{\sqrt{k}}{\beta^*\omega d},\frac{500\nu}{d^2\omega}\right),\frac{4\rho\sigma_{\omega 2}k}{CD_{k\omega}d^2}\right]\right\}^4 \quad (6)$$

$$CD_{k\omega}=\max\left(2\rho\sigma_{\omega 2}\frac{1}{\omega}\frac{\partial k}{\partial x_j}\frac{\partial\omega}{\partial\omega j},10^{-10}\right) \quad (7)$$

and $\nu_t=\mu_t/\rho$ is the turbulent kinematic viscosity, μ_t is computed as:

$$\mu_t=\frac{\rho a_1 k}{\max\left(a_{1\omega},\Omega F_2\right)} \quad (8)$$

$$F_2=\tanh\left[\max\left(2\frac{\sqrt{k}}{\beta^*\omega d},\frac{500\nu}{d^2\omega}\right)\right]^2 \quad (9)$$

where d is the distance between the field point and the nearest wall, and Ω is the vorticity magnitude.

Turbulence model constants are as following $\sigma_{k1} = 0.85034, \sigma_{k2} = 1.0$, $\sigma_{\omega 1} = 0.5$, $\sigma_{\omega 2} = 0.85616$, $\beta_1 = 0.075$, $\beta_2 = 0.0828$, $\beta^* = 0.09$, $a_1 = 0.31$, $\gamma_1 = 5/9$ and $\gamma_2 = 0.4403$ [15, 16].

Displacement of the pile is estimated by the equation of motion which is expressed as:

$$m\frac{d^2Z}{dt^2} + c\frac{dZ}{dt} + kZ = F_z \qquad (10)$$

where Z is the displacement of the cylinder in cross-flow direction, F_z is the lift force on the cylinder, m, c and k are the mass, damping coefficient and the spring constant of the system, respectively. The added mass is taken into account when calculating the pile mass. Damping (c) and pile stiffness (k) are considered based on the study of Angrilli and Cossalter [3].

The free surface is traced by the VOF technique [17]. The Finite Volume Method was employed to solve the governing equations of the flow and transport equation for the volume fraction of water, in which the equations are integrated on the control volume and time.

2.2. Computational Domain and Boundary Conditions

To simulate the wave-pile interaction in a wave flume, the computational domain was a rectangular box which is occupied by water, air and the pile. The dimensions of the wave flume at the horizontal plane were 26.5 × 0.6 m and 0.8 m high so that free surface of the waves could easily pass through the flume without colliding with the ceiling. The diameter of both piles was 4 cm with square and circular cross-sectional shape. Figure 1 shows a schematic view of the wave flume with a circular pile as well as boundary conditions which were selected in the simulation. As seen, in the bed of the flume, the boundary condition is assumed to be no-slip as all components of the flow velocity are nil. The ceiling of the wave flume and its lateral walls (front and back in OpenFOAM modelling) are considered as the slip wall boundaries [10].

The wave inlet is to the left of the flume where regular waves are generated and propagated. At the outlet, a wave attenuation technique (relaxation zone) was applied that sufficiently prevented the reflection of the waves in the wave flume [16]. The pile was set 14 meters from the inlet boundary and the non-slip wall boundary condition was applied with a smooth hydraulic surface. The wave2Foam toolbox was applied to generate and propagate free surface water waves. Waves2Foam uses the VOF technique for free surface tracking [10]. It also prevents the reflection of waves in the flume by creating a relaxation zone (active sponge layers). This toolbox was created using the above in a multi-phase "InterDyMFoam" solver with dynamic mesh functionality. In this study, the pile is free to vibrate in the transverse direction of flow (cross-flow) and it was restrained from in-line vibration. To do so, the dynamic mesh was applied in the simulation.

Mesh generation in the computational domain was performed using the "blockMesh" tool. In this process, the computational domain was divided into 12 blocks and 476,800 hexagonal computing cells. As the pile and bed approached, smaller computational cells were applied to capable the model to account for the full impact of the wall boundary on the simulation. Numerical modelling was performed with different forms of meshing to obtain the optimum state. The results of the present model are not very sensitive to the form and dimensions of the computational cells. Figure 2 shows a view of the applied mesh for both circle and square cross-sectional shape pile.

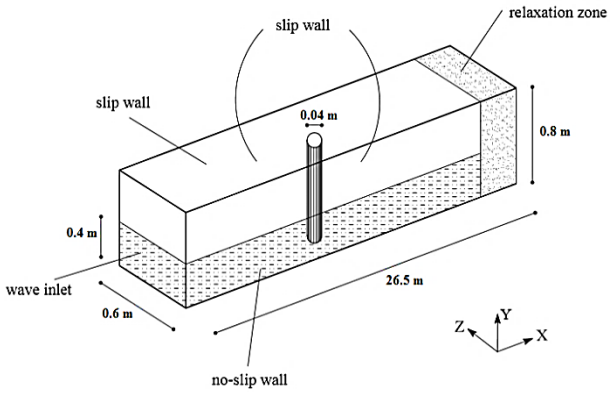

Figure 1. Computational domain and boundary conditions (not scale)

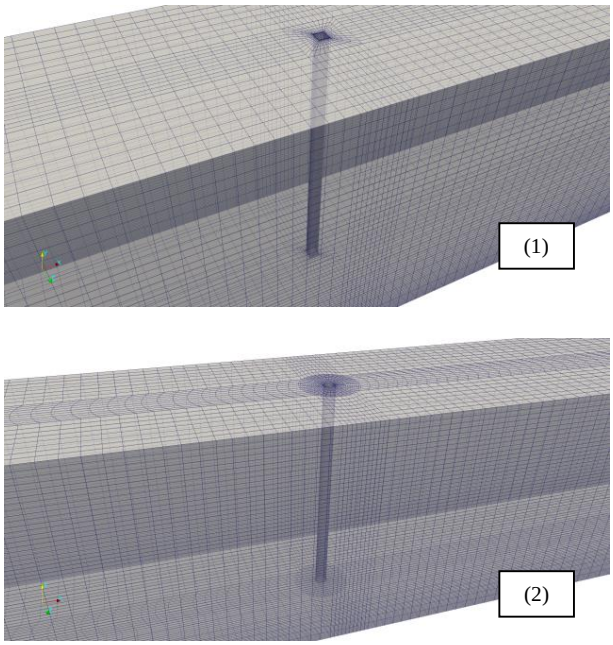

Figure 2. A view of the 3D applied mesh around the pile, (1) square cross-section, (2) circle cross-section

3. Model Validation

The numerical model validated by comparison of results against experimental data of Mo et al. [8]. These experiments conducted in the Large Wave Flume (GKW), with an effective length of 309 m and a width of 5 m, belonged to the Coastal Research Centre (FZK) in Hannover, Germany. A steel circular cylinder with a diameter of 70 cm was installed in 40 m away from the wave maker (left boundary). All the experimental conditions were numerically modelled but the wave flume length was considered equal to 77 m to reduce the computational costs. The experiment characteristics are shown in Table 1.

Table 1: The experiment characteristics

Wave Type	Water depth (*d*) [m]	Wave Height (*H*) [m]	Wave period (*T*) [sec]	KC Number [-]
Regular	4.76	1.20	4	6.13

The mesh generation was carried out by using the "blockMesh". The computational domain was discretized by eight-node hexahedron cells. Finer cells were used at the edge of the cylinder in order to simulate the large velocity gradients there. A total number of 433000 cells were used in computational domain. Boundary conditions were as they were in the section 2. Calculations were carried out for physical duration of 40 sec (10 waves passed over the pile), and then the outcomes were evaluated. Several model outcomes were compared to the experimental data to validate the numerical model.

The time history of the horizontal component of water particle velocity at points along the side wall of the flume along the pile at two different depths (y/d= -0.32 and y/d= -0.57, y is the distance from still water level and d is the water depth) have been plotted against the corresponding values measured in the experiment in Figure 3. As can be seen at both depths, there is an acceptable agreement between the model results and the experimental data.

Figure 4 shows the time history of the total in-line force applied to the pile against the corresponding experimental results. The force has been obtained from the sum of the pressure and viscous stresses on the wetted surface of the pile at each time step. As can be seen, there is an excellent agreement between the results of the simulation and those of the experiment. This means that the numerical model can predict well the hydrodynamic forces exerted on the pile.

The dynamic pressure was extracted at six points with different angles at a specific depth (y/d= -0.11) around the pile during the simulation and was plotted against the corresponding experimental data in Figure 5. The agreement between the experimental data and the numerical results for this case are extremely good. Given that the vortices generated around the pile affect the pressure field, by obtaining the correct values of the pressure field, it is expected that the numerical model can predict the vortex dynamics well.

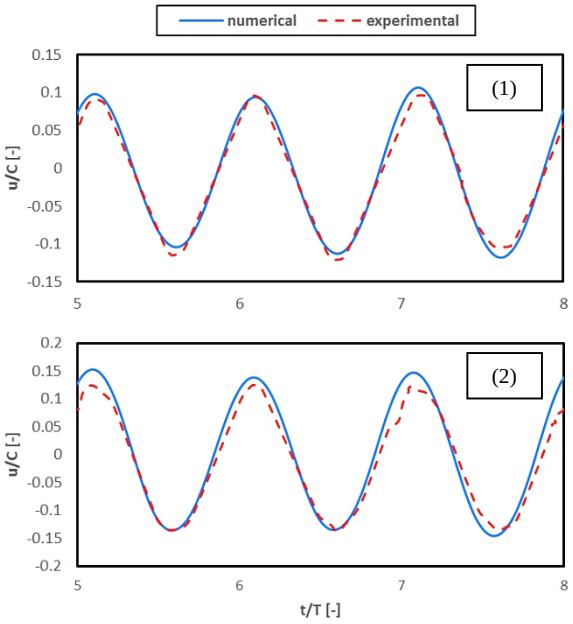

Figure 3. The horizontal component of water particle velocity at points along the side wall of the flume along the pile at two different depths (1) y/d= -0.57 (2) y/d= -0.32

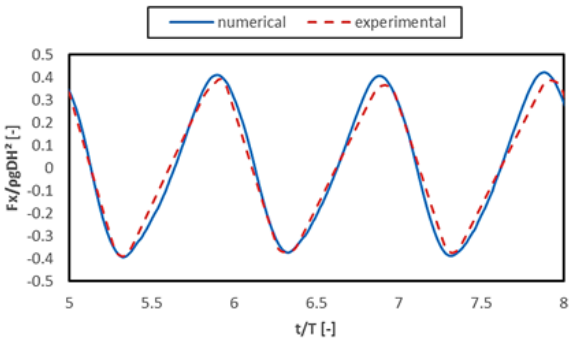

Figure 4. Time history of the total in-line force applied to the pile against the corresponding experimental results

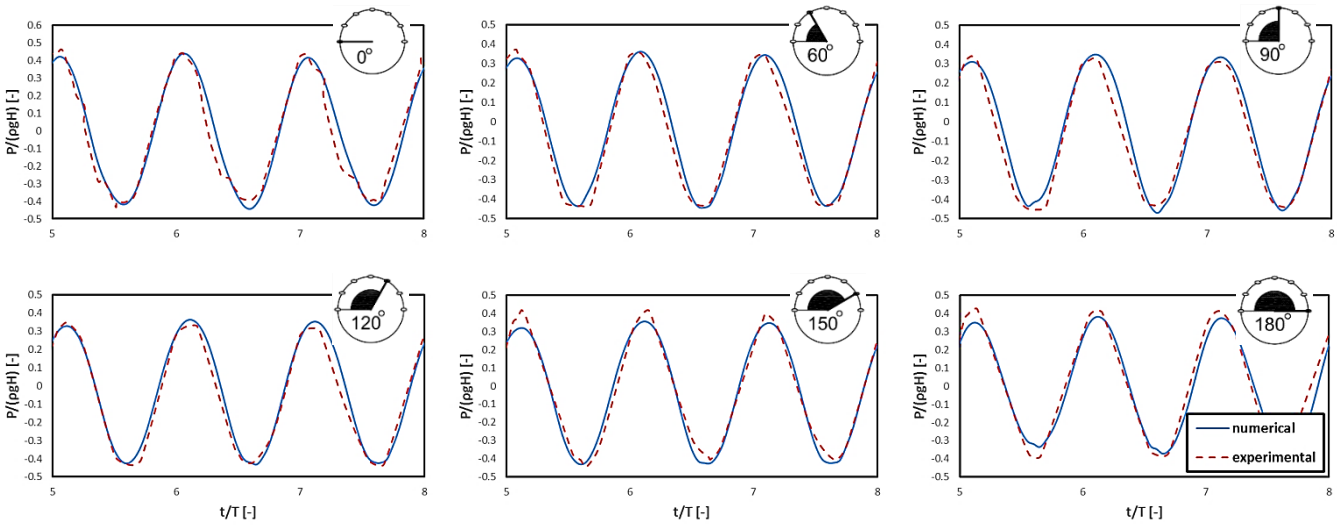

Figure 5. The dynamic pressure at six points with different angles at the depth of *y/d*= -0.11 around the pile

4. Results and Discussion

To investigate the impact of cross-sectional shape on vortex shedding and pile vibration, wave characteristics of two experimental studies [19, 20] were selected to consider varying vortex shedding regimes. Each wave characteristics was modelled with circular and square pile separately. In order to obtain the dynamic behavior of the pile, simulations were continued for the physical duration of 20 wave period. All aspects of numerical method including consistency, stability, convergence, accuracy and mesh dependency on the results were considered during the simulations.

Wave and pile characteristics which were applied in the numerical model are presented in Table 2. As seen, the pile and wave characteristics belong to KC=6.1 and KC=20.1 regimes. When KC=6.1 vortex shedding is in its early stage for the circular pile. In this regime, one vortex is shed in each half-period of the waves and the attached vortices are washed around the pile when the flow reverses. In the case of square pile no vortex shedding occurs when KC<11 [21]. For another case, when KC=20.1, vortex shedding is completely developed for both cross-sectional shapes. In this regime, two vortices are shed in each half-period of the waves. The attached vortices are washed around the pile when the flow reverses, in the same way as in the previous regimes [19].

Q criterion is a method that can be applied to investigate vortex shedding [22]. Figure 3 shows *Q* criterion for circular and square pile when KC=6.1. In the figure, wave-induced flow is from left to right which is called crest half period and ωt=90º. As seen, when KC=6.1 vortex shedding was in its early stage for circular pile but for the square pile only lee wake vortices were generated and no shedding occurred.

Table 2: Wave and pile characteristics applied in the numerical model

Pile Section *D*=4 [cm]	Water depth (*d*) [m]	Wave Height (*H*) [m]	Wave period (*T*) [sec]	KC Number [-]	Pile Reynolds Number [-]
D	0.4	0.023	4.4	6.1	2200
	0.4	0.126	2.6	20.1	12400
D	0.4	0.023	4.4	6.1	2200
	0.4	0.126	2.6	20.1	12400

Figure 4 and 5 show vorticity magnitude around circular and square pile when KC=6.1 and KC=20.1 respectively. The figure was depicted when pile is in the crest half period (ωt=90º). According to figure 4, some concentration in vorticity was seen in front of the sharp edges of the square pile. Also, the magnitude of vorticity was diminished over the side surfaces of the square pile between sharp edges. In circular Pile case, vorticity distribution was on the two lateral edges of the pile and also its magnitude was larger compared to that of the square pile.

As seen in figure 5 (when KC=20.1), vorticity pattern around the circular pile and square pile varies entirely. In square pile case, vorticity concentration in front of the sharp edges of the pile caused that vorticity magnitude and distribution of that would be quite different compared to those of the circular pile. Since the adverse pressure gradient generated in front of the square pile is larger than that generated in front of the circular pile. These results are in line with experimental observations [19].

Figure 6 illustrates the lift force coefficient (C_l) for square and circular pile when KC=20.1 and KC=6.1 during two wave periods. Lift force is acting on the pile in the transverse direction of flow and its coefficient is obtained by:

$$C_l = \frac{F_z}{0.5\rho U^2 D} \quad (11)$$

where ρ is the water density, U denotes the flow velocity and D is the pile diameter. F_z is the lift force which is predicted by integrating the pressure and viscous stresses in cross-flow direction along the pile in a discretized manner. The pressure and viscous forces from each cell face on the surface of the pile are summed to find the total pressure and viscous forces, respectively. As seen in Figure 6, when KC=20.1 for square pile lift coefficient was quite larger than that of the circular pile. Whereas, for KC=6.1 small difference of lift coefficient between square and the circular pile was seen which can be attributed to asymmetry in vortices around the pile. Consequently, the cross-sectional shape has an influence on the resulting force.

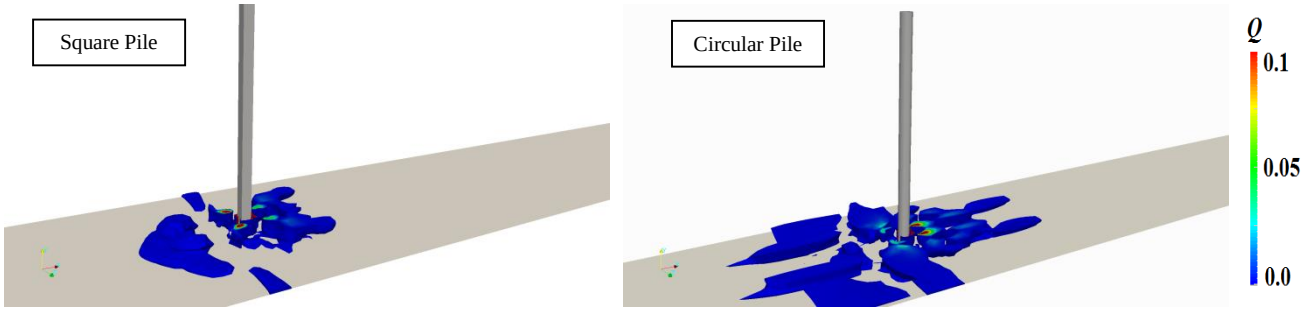

Figure 3. *Q* criterion around the square and circular pile in crest half period (ωt=90°) for KC=6.1

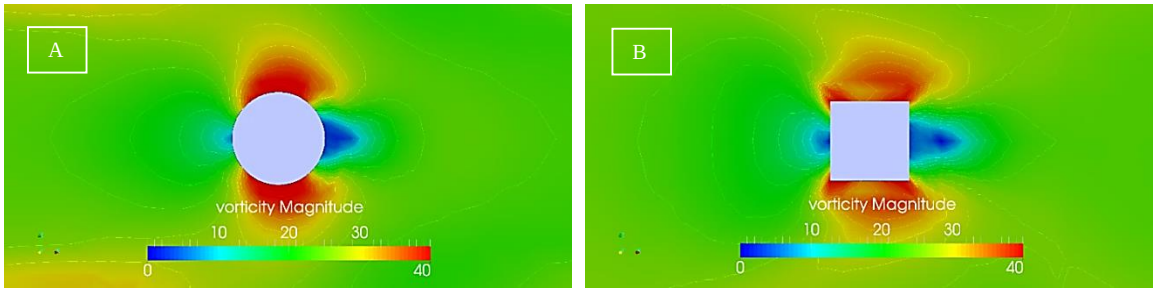

Figure 4. Vorticity magnitude contour around circular (a) and square (b) pile in crest half period (ωt=90°) for KC=6.1

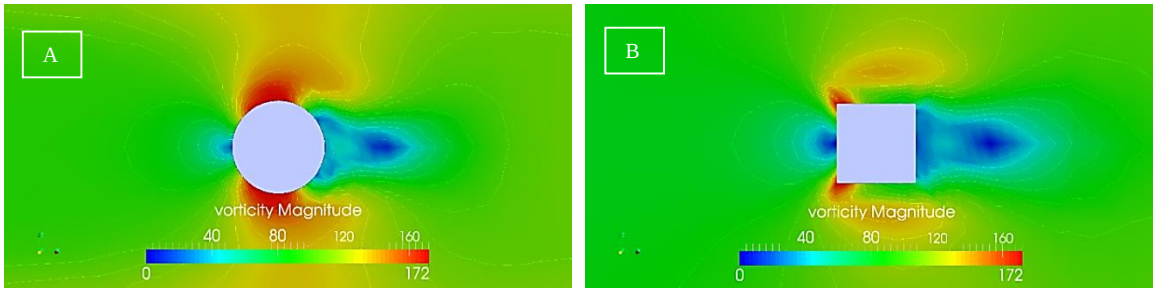

Figure 5. Vorticity magnitude contour around circular (a) and square (b) pile in crest half period (ωt=90°) for KC=6.1

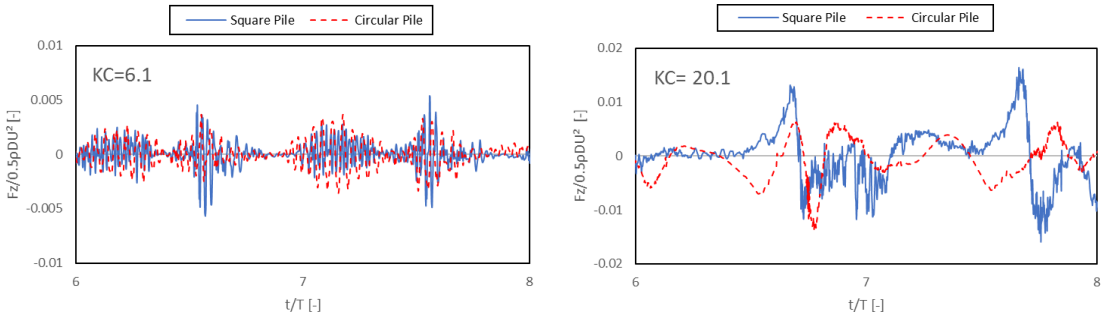

Figure 6. Time series of lift coefficient (c_l) for square and circular pile when KC=6.1 and KC=20 during two wave periods

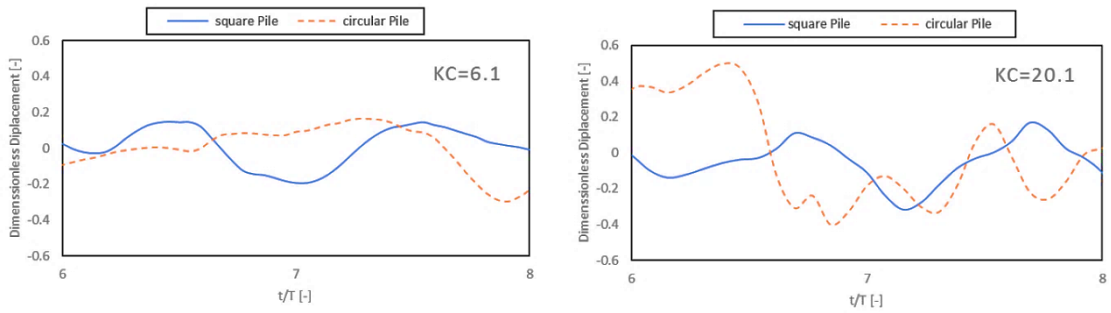

Figure 7. Time series of pile displacement for square and circular pile when KC=6.1 and KC=20 during two wave periods

The fluctuation of lift force can be attributed to the vortex shedding or asymmetry in vortices generated around the pile [7]. When KC=20.1 vortex shedding pattern is different between square and circular cross-section pile. Consequently, a phase difference was seen in the lift force between square and circular cross-section shapes. The difference in the lift coefficient between the square and the circular pile for each of the cases when KC=6.1 or KC=20.1 can be justified by the difference in vortex dynamics around the pile, which was explained above. In addition, the fluctuation of the lift coefficient differs between these two cross-sectional shapes. It was seen that when KC=20.1 lift force frequency of circular pile case is quite larger than that of square pile case. It must be noted that in this study the flow is due to wave which is a complicated flow field around the pile. In wave-induced flow around the pile, the lift force frequency is not the same as vortex shedding frequency [7].

Displacement of both pile during two wave periods for KC=6.1 and 20.1 is depicted in Figure 7. As seen, for both square and circular cross-section, the number of pile oscillation increased by increasing KC number. This may be due to that by increasing of KC number lift force frequency increases, causing the pile to oscillate [7]. In addition, the amplitude of pile oscillation increased by increasing KC number for both cross-sectional shapes. This can be the result of increasing the lift force magnitude by increasing the KC number.

Figure 8 shows power spectral density (PSD) from lift coefficient, which is obtained by Fourier transform of that, versus Strouhal number (St) for square and circular pile when KC=20. Strouhal number (St) is a dimensionless number describing oscillating flow mechanisms which is stated by the following equation:

$$\mathrm{St} = \frac{f_v D}{U} \tag{11}$$

where U is the fluid velocity, f_v is the vortex shedding frequency, and D is the pile diameter. The pick of PSD for square and circular pile denotes the Strouhal number. This method is applied to obtain vortex shedding frequency [21]. As seen from the figure, Strouhal numbers (St) are 0.19 and 0.2 for the square pile and circular pile, respectively. It was concluded that the frequency of the vortex shedding for circular pile was 1 percent larger than that of the square pile in this regime of KC. The frequency of the lift force can depend on the vortex shedding frequency (f_v). Therefore, it can be expected that the vortex shedding frequency in the circular pile case should be larger compared to the square pile case.

In this study pile is free to vibrate in the transverse direction of flow; hence, vortex-induced vibration (VIV) of the pile is probable. In pile-structure problems, VIV has been always of great interest. In this condition, Reduced Velocity (V_r) would be important which is stated by the following equation:

$$\mathrm{V_r} = \frac{U}{f_m D} \tag{12}$$

where f_m is the Eigen frequency of the pile and other parameters are the same as mentioned above. When f_m is close to f_v, the lock-in or synchronization occurs, which means that $V_r \approx 1/\mathrm{St}$. In this case, the vortex shedding frequency becomes equal to the Eigen frequency of the pile. The vibration amplitude is the maximum, and the correlation between the excitation forces along the span increases dramatically [23].

Figure 9 and 10 illustrate power spectral density (PSD) of the pile displacement over the frequency of vibration when KC=20.1 and KC=6.1 respectively. In this case, the frequencies of vibration for square and circular pile were quite close together. According to figure 9 and 10, by calculating V_r of each case, it was concluded that none of the cases were in the lock-in region.

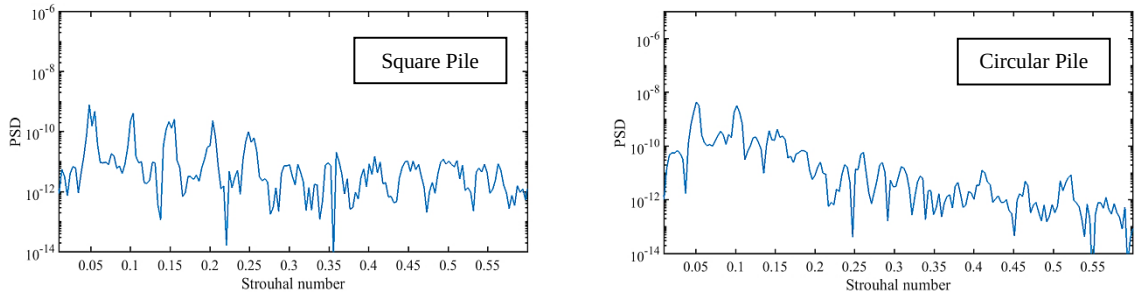

Figure 8. Power spectral density (PSD) of lift coefficient versus Strouhal number (St) for square and circular pile when KC=20.1

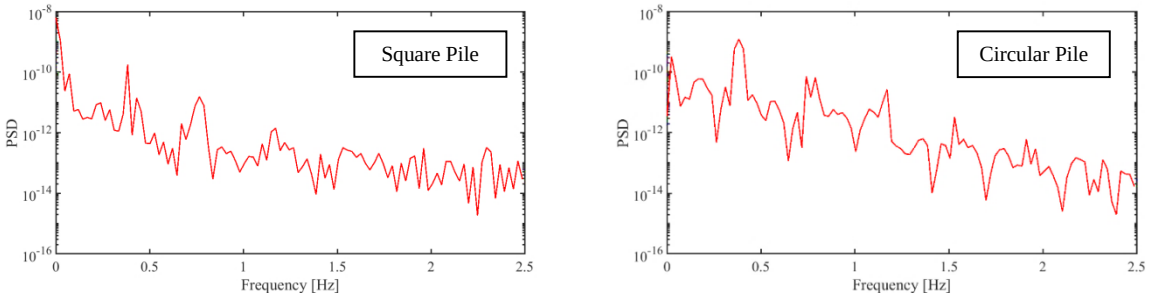

Figure 9. Power spectral density (PSD) of pile displacement over frequency for the square and circular pile when KC=20.1

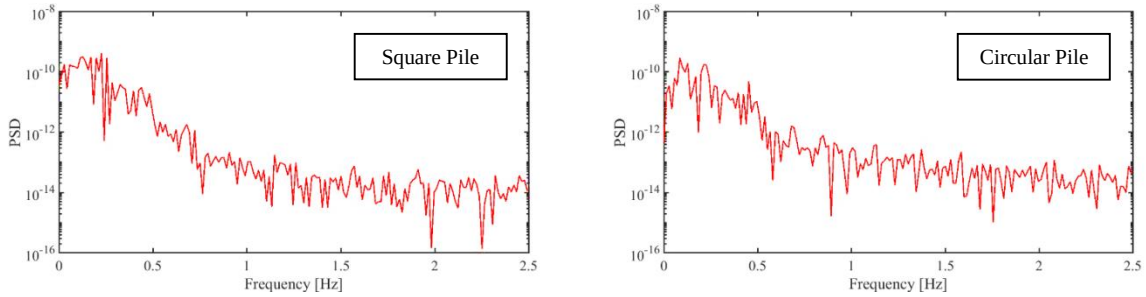

Figure 10. Power spectral density (PSD) of pile displacement over frequency for square and circular pile when KC=6.1

5. Conclusions

Three-dimensional numerical simulation of regular waves passing over a square and circular pile has been carried out in order to investigate vortex dynamics as well as vortex-induced vibration. OpenFOAM was employed as an open source tool of computational fluid dynamics (CFD) involving a solver capable of modeling the multi-phase Eulerian method for simulating rectangular wave flume and monopile. RANS equations to solve flow field together with motion equation to capture structure response were applied. The free surface was traced by the VOF method. Meshes are totally hexahedral and were created using the "blockMesh" utility. Mesh deformation was applied to capture the pile displacement due to cross-flow vibration.

Some numerical model results were compared to the experimental data to validate model e.g. the time history of the horizontal component of water particle velocity at at points along the side wall of the flume along the pile at two different depths, the time history of the total in-line force applied to the pile and the time history of the dynamic pressure at six points with different angles at a specific depth around the pile.

Computations were done for 4 cases with two numbers of Keulegan-Carpenter (KC) and two of the cross-sectional shape. Every model was run for the physical duration of 20 wave period to converge. Investigations were carried out on the vorticity, *Q* criterion and lift force coefficient and the following results were obtained:

- Vorticity magnitude around the pile was depicted and it was seen that when KC=6.1 concentration of vorticity was increased in sharp edges of the square pile.
- When KC=20.1 the vortex pattern was completely different between the square pile and the circular pile, which may be due to the difference of the adverse pressure gradient created against the square pile compared to the circular pile.
- When KC=20, the lift coefficient is larger for square pile compared to the circular pile. When KC=6.1 small difference of lift coefficient between square and the circular pile was seen.

- By observing the pile displacement it was seen that for both square and circular cross-sectional shape, the number of pile oscillation increased by increasing KC number.

From the Fourier transform and power spectral density (PSD) from lift force coefficient and pile displacement it was concluded that:

- Strouhal number for the circular pile was a bit larger and consequently, vortex shedding frequency was larger too compared to the square pile.
- Pile displacement over frequency was investigated and it was seen that when KC=20.1, vibration frequency of square and circular pile were close together.

8. References

1- Sarpkaya, T. and Rajabi, F. (1979), *Dynamic response of piles to vortex shedding in oscillating flows*, Offshore Technology Conference.

2- Zedan, M.F., Yeung, J.Y., Salane, H.J. and Fischer, F.J. (1981), *Dynamic response of a cantilever pile to vortex shedding in regular waves*, Journal of Energy Resources Technology, Vol. 103(1), p. 32-40.

3- Angrilli, F., Cossalter, V. (1982), *Transverse oscillations of a vertical pile in waves*, Journal of Fluids Engineering, Vol. 104(1), p. 46-52.

4- Bearman, P.W., 1984. *Vortex shedding from oscillating bluff bodies*, Annual review of fluid mechanics, Vol. 16(1), p. 195-222.

5- Griffin, O.M. (1985), *Vortex shedding from bluff bodies in a shear flow: a review*, Journal of Fluids Engineering, Vol. 107(3), p. 298-306.

6- Blevins, R.D. (1990), *Flow-induced vibration*. Van Nostrand Reinhold. New York, Vol. 199(0).

7- Sumer, B.M. (2006), *Hydrodynamics around cylindrical strucures* (Vol. 26), World Scientific.

8- Downes, K. and Rockwell, D. (2003), *Oscillations of a vertical elastically mounted cylinder in a wave: imaging of vortex patterns*, Journal of Fluids and Structures, Vol. 17(7), p. 1017-1033.

9- Mo, W., Irschik, K., Oumeraci, H. and Liu, P.L.F. (2007), *A 3D numerical model for computing non-breaking wave forces on slender piles*, Journal of Engineering Mathematics, Vol. 58(1-4), p. 19-30.

10- Jacobsen, N.G., Fuhrman, D.R. and Fredsøe, J. (2012), *A wave generation toolbox for the open-source CFD library: OpenFoam®*, International Journal for Numerical Methods in Fluids, Vol. 70(9), p. 1073-1088.

11- Kasvaei, M.M.B., Kazeminezhad, M.H. and Yeganeh-Bakhtiary, A. (2017), *Numerical Investigation on Wave Induced Vortex Dynamics Around Cylindrical Pile with Considering Varying Keulegan-Carpenter Number*, In ASME 2017 36th International Conference on Ocean, Offshore and Arctic Engineering (pp. V07AT06A059-V07AT06A059).American Society of Mechanical Engineers.

12- Lou, M., Dong, W. and Guo, H. (2011), *A vortex induced vibration of marine riser in waves*, Acta Oceanologica Sinica, Vol. 30(4), p. 96.

13- Zhao, M. and Cheng, L. (2014), *Vortex-induced vibration of a circular cylinder of finite length*, Physics of Fluids, Vol. 26(1), p. 015111.

14- Menter, F.R. (1994). *Two-equation eddy-viscosity turbulence models for engineering applications*, AIAA journal, Vol. 32(8), p. 1598-1605.

15- Wilcox, D.C. (1988), *Reassessment of the scale-determining equation for advanced turbulence models*, AIAA journal, Vol. 26(11), p. 1299-1310.

16- Amini Afshar, M. (2010), *Numerical wave generation in Open FOAM®*, PhD thesis, Chalmers University of Technology.

17- Hirt, C. W., & Nichols, B. D. (1981), *Volume of fluid (VOF) method for the dynamics of free boundaries*, Journal of computational physics, Vol.39(1), p. 201-225.

18- Mohammad Beigi Kasvaei, M., Kazeminezhad, M.H. and Yeganeh-Bakhtiary, A. (2018), *Numerical Study on Hydrodynamic Force and Wave Induced Vortex Dynamics around Cylindrical Pile*, International Journal of Coastal and Offshore Engineering, Vol.2(4), p. 1-11.

19- Sumer, B.M., Christiansen, N. and Fredsøe, J. (1997), *The horseshoe vortex and vortex shedding around a vertical wall-mounted cylinder exposed to waves*, Journal of Fluid Mechanics, Vol.332, p. 41-70.

20- Dey, S., Sumer, B.M. and Fredsøe, J. (2006), *Control of scour at vertical circular piles under waves and current*, Journal of Hydraulic Engineering, Vol. 132(3), p. 270-279.

21- Sumer, B. M., Christiansen, N., & Fredsøe, J. (1993), *Influence of cross section on wave scour around piles*, Journal of waterway, port, coastal, and ocean engineering, Vol.119(5), p. 477-495.

22- Chen, Q., Zhong, Q., Qi, M., and Wang, X. (2015), *Comparison of vortex identification criteria for planar velocity fields in wall turbulence*, Physics of Fluids, Vol. 27(8), p. 085101.

23- Le Cunff, C., Biolley, F., Fontaine, E., Etienne, S. and Facchinetti, M.L. (2002), *Vortex-induced vibrations of risers: theoretical, numerical and experimental investigation*, Oil & Gas Science and Technology, Vol. 57(1), p. 59-69.